Available online at www.sciencedirect.com
ScienceDirect
C. R. Mecanique 335 (2007) 315–322
COMPTES RENDUS MECANIQUE
http://france.elsevier.com/direct/CRAS2B/

Melting and solidification: processes and models/Processes and control of crystal growth

Theoretical confirmation of the crystallization of a compound alloy using the AHP crystal growth method

Marina Marchenko

Center for Thermophysical Researches "Thermo" Ltd, Alexandrov, Vladimir Region, 601650, Russia

Abstract

The crystallization of $In_xGa_{1-x}Sb$ for $x = 0.06$ by the AHP-method (Axial Heat flux, close to the Phase interface) is considered. Heavy indium is rejected during crystal growth close to the interface. Indium significantly decreases the crystallization temperature, and has an influence on the melt convection. The AHP-heater serves as a partition; due to this partition a small well-mixed liquid zone with high In concentration exists and causes a stable crystal growth with high composition after the crucible is moved down. The grown crystal is very homogeneous. Numerical modelling has also been performed, using finite difference schemes. ***To cite this article: M. Marchenko, C. R. Mecanique 335 (2007).***

Résumé

Confirmation théorique de la cristallisation d'un alliage composite utilisant la méthode AHP. La croissance cristalline du $In_xGa_{1-x}Sb$ pour $x = 0{,}06$ par la méthode AHP (flux de chaleur axial proche de l'interface) est considérée. L'indium lourd est rejeté près de l'interface pendant la croissance du cristal. L'indium réduit de manière significative la température de cristallisation, et influence la convection dans le bain fondu. Le réchauffeur-AHP agit comme une cloison. En raison de cette cloison une zone réduite de liquide bien mélangé avec une haute concentration d'In existe et assure la croissance stable du cristal avec une composition élevée après déplacement du creuset vers le bas. Le cristal obtenu est très homogène. Un modèle numérique basé sur la méthode des différences finies a été également développé. ***Pour citer cet article : M. Marchenko, C. R. Mecanique 335 (2007).***

Keywords: Computational fluid mechanics; Thermal and solute convection; Transitions; Interface; Phase change diagram

Mots-clés : Mécanique des fluides numérique ; Convection thermo-solutale ; Transitions ; Interface ; Diagramme de phase

1. Introduction

Conventional ternary compound semiconductor alloys are traditionally grown epitaxially on single crystal substrates of binary compounds (such as GaAs, GaSb, InP, GaP) with discrete lattice constants, so there is a detrimental lattice mismatch between the substrate and the device layers. Bulk substrates of ternary compound semiconductors could solve this problem and also open up numerous possibilities of interesting band gap engineering in homo- and hetero-epitaxial devices. In [1] it was mentioned that the main problem in the growth of $In_xGa_{1-x}Sb$ crystals is a

E-mail address: marchenko_marina@sbcglobal.net.

1631-0721/$ – see front matter
doi:10.1016/j.crme.2007.05.012

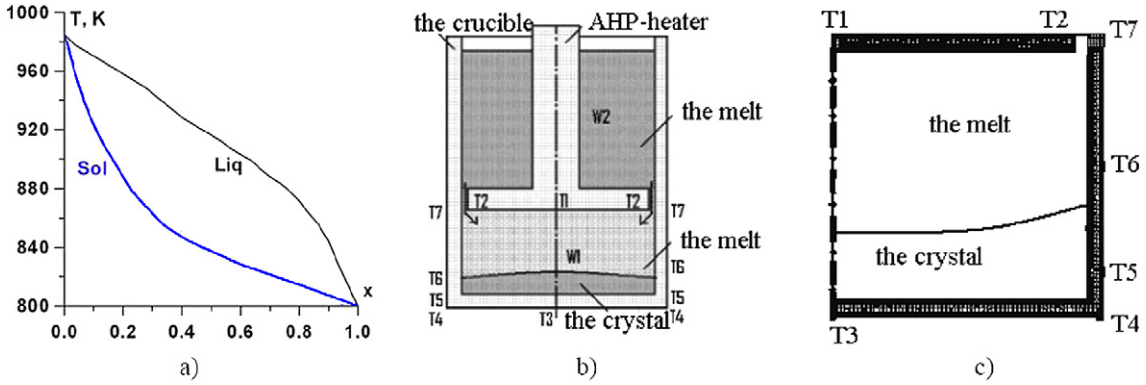

Fig. 1. (a) Phase diagram, upper curve is liquid composition, lower curve—solid composition; (b) the schematic of the AHP-method, where the points marked T1–T7 are positions of the thermocouple placements; (c) the physical domain for numerical modeling.

Fig. 1. (a) Diagramme de phase, courbes de dessus composition liquide, courbes de dessous—composition solide ; (b) schéma de la méthode AHP, T1–T7 placements des thermocouples ; (c) domaine de calcul.

combination of high concentration and the large liquid/solid interval in the phase diagram (Fig. 1(a), see also [2]). Experiments described in [1] demonstrate strong axial and radial chemical segregation: grown crystals are generally heterogeneous and cracked (even for an initial melt composition $x = 0.06$ and internal radius 6 mm). The diffusion coefficient is practically unknown for this type of material, but some approximation for the dependence of the diffusion coefficient on melt concentration has been suggested [3]. The temperature regime, system geometry and initial melt composition of the experiment from [1] were used for numerical modeling in [4], where the dependence of the diffusion coefficient on concentration used was similar that of [3]. As was shown in [4], numerical results and experimental data concerning shape and interface positions, and the grown crystal composition, are in good agreement. The mathematical model presented in this article has been applied to the crystallization of InGaSb [4].

The AHP-method [5,6] is a modification of the Bridgman growth, where an additional heater (or baffle) is submerged into the melt. As usual, thermocouples are placed into the crucible side wall, in the crucible bottom and in the AHP-heater. It is expedient to consider, in mathematical model, a geometrical region enclosed between the thermocouples. The experiment of InGaSb crystal growth by the AHP-method without seed from a compound melt and its numerical simulation were presented in [7,8], where a very homogeneous crystal was grown with radius equal to 23 mm. In the present article, the test case problems are considered. Therefore, some idealized boundary conditions close to the experimental data are taken into account in order to investigate features of crystal growth. The graphite crucible was modeled with an internal radius of 10 and 30 mm. The influence of submerged heater and temperature regimes on melt flow and concentration distribution in grown crystal was shown in [9]. The radius of 10 mm was chosen in order to have some comparison between numerical results (AHP- and Bridgman methods) and the results of the experimental Bridgman crystal growth process [1]. The temperature distribution was changed with gradient of 60 K/cm along the crucible side wall (close to conditions of the experiment from [1]). When the crucible is moved down with velocity V, the melt from the upper part ($W2$) above the AHP moved down through the gap between AHP-heater and crucible (see Fig. 1(b)). The computational region is presented at Fig. 1(c). The lower part, together with the crucible and the grown crystal were increased during the growth process.

Transient crystal growth problems are considered in the axisymmetrical configuration. The movement of the incompressible viscous liquid in the melt zone, driven by both temperature and concentration gradients, was considered by solving the Navier–Stokes equations written in a vorticity–stream function formulation, using the Boussinesq approximation. In the melt zone, both heat and solute transport were considered. At the melt/crystal (m/c) interface, the equilibrium temperature, liquid and solid compositions were connected by the phase change diagram. A small supercooling effect from the equilibrium temperature was allowed at the interface for the case of the phase diagram [4,10]. The kinetic coefficient of rough growth has been chosen at a large value as was described in [11]. The instantaneous solidification velocity was calculated, proportional to interface supercooling. The temperature equation was solved in the zones of crystal; crucible wall and bottom of AHP-heater (see Fig. 1(c)). The boundary condition of the vertical component of the flow velocity in a gap was defined by mass balance. It is implied that the upper melt zone was well mixed and had a concentration equal initially to one, and that return flow to the upper zone was absent. The symmetry

condition was considered for concentration at the axis, the equality to zero for the flow of concentration was imposed on the crucible wall and on the bottom of AHP heater.

The software tool 'KARMA1' [12] with some modifications was used for the numerical simulation as in [4] and [10]. At each time step both liquid and solid areas are mapped into square blocks. Finite-difference schemes were used for approximation of equations [12]. A non-uniform mesh was used for all blocks. In each block the mesh was clustered near the boundaries, especially near the liquid zone boundaries. An implicit, conservative, monotonic, unconditionally stable different schemes, based on extended stencils with monotonizing regularizers of the third order, were used to approximate the equations and boundary conditions [13]. All algebraic equations were combined into two systems. One of these consists of the vorticity and stream function, together with boundary conditions; another is temperature and concentration equations with boundary conditions and conditions at the m/c interface. Due to such a combination it is possible to uniformly solve any kind of crystal growth problem: either from a pure melt or one with dopant added, or from a high compound alloy [14], or facet growth [15]. In [12] all equations had been combined into three systems: vorticity and stream function, temperature, and concentrations. Such partitions were required because of the shortage of computer capacity a few years ago. Now this weakness has been overcome.

In the present article it is numerically demonstrated that it is possible to grow an $In_xGa_{1-x}Sb$ crystal with composition close to $x = 0.06$ with good quality: very homogeneous both in lateral and in longitudinal directions. Such results are based on the analysis of the crystallization dynamics and on the study of melt convection.

2. Crystal growth

In this article, a numerical investigation of bulk $In_xGa_{1-x}Sb$ crystal growth by the AHP method [5,6] is reported. As mentioned earlier, experiments from [1] showed that even for a small radius of 6 mm and melt composition $x = 0.06$, the crystals grown are very heterogeneous. During crystallization, the heavy indium was rejected and accumulated close to melt/crystal (m/c) interface. The intensity of melt convection was decreased due to the influence of a solute convection. Also the crystallization temperature was decreased and varied along the radius. A heavy concentration of In was accumulated close to the axis of the interface. The m/c interface concavity inside the crystal reached as high as 8 mm (see [1,3,4]). The diffusion coefficient is not well known [3]. The dependency of the diffusion coefficient on concentration, used in [3] and [4], is very similar; it decreased with increasing indium concentration under conditions of low diffusivity, and the slow convection heterogeneity of grown crystal increased.

Fig. 1(b) represents the schematic of the AHP method: an additional heater (or baffle) is submerged into the crucible with the melt. The seed is placed in the crucible bottom. The zone $W1$ between the seed and the AHP-heater has an initial concentration c_1. It is implied that the melt in the upper zone $W2$ is well mixed and that its composition is equal to c_2. When the crucible is moved down with a velocity V, the fresh melt flows into the crystallization zone ($W1$) through the small gap of 0.5 mm between the AHP-heater and the crucible. The AHP-heater can also move up with velocity V. Thermocouples are placed at the crucible side wall, at the crucible bottom and inside the AHP-heater's bottom. The geometrical region subjected to mathematical modeling is shown in Fig. 1(c).

The transient crystal growth problem is considered in an axisymmetrical configuration. The movement of the incompressible viscous liquid in the melt zone, driven by both temperature and the concentration gradient, was considered by solving the Navier–Stokes equations written in a vorticity–stream function formulation, using the Boussinesq approximation. In the melt zone both heat and solute transport were considered. At the m/c interface the equilibrium temperature, the liquid compositions and the solid compositions were connected by a phase change diagram. A small supercooling effect from the equilibrium temperature was allowed at the interface for the case of the phase diagram [4,10]. The kinetic coefficient of the rough growth has been chosen as a large value, as was described in [11]. The instantaneous solidification velocity was calculated, proportional to the interface supercooling. The temperature equation was solved in the zones of the crystal, in crucible wall and at the bottom of the AHP-heater (see Fig. 1(c)). The boundary condition of the vertical component of the flow velocity in a gap was defined by mass balance. It was implied that the upper melt zone was well mixed and had a concentration equal to the initial one, and return flow to the upper zone was absent. The symmetry condition was considered for concentration at the axis, zero flow of concentration was imposed on the crucible wall, and on the bottom of AHP heater.

In the present study, the crystallization dynamics and features of flow convection have been investigated for problems of growing $In_xGa_{1-x}Sb$ crystals by the AHP method and the Bridgman technique. The possibility of heterogeneous crystal growth by the AHP-method is demonstrated.

3. Mathematical model and method

The geometrical domain of simulation is presented in Fig. 1(c). The left boundary of the geometrical region is the z-axis; the crystal regions and the melt regions, together with the phase change boundary, were calculated at each time step. The crystal growth experiment was modeled using a two-dimensional cylindrical (r, z) coordinate system with the origin located at the bottom of the crucible.

The non-dimensional numbers Grasshoff (Gr), Prandtl (Pr), Schmidt (Sc), Stephan (St) and Peclet (Pe) numbers are defined as:

$$Gr = \beta_{\mathrm{T}} g R_c^3 \Delta T/\nu^2, \qquad Gr_{\mathrm{d}} = \beta_{\mathrm{c}} g R_c^3 \Delta c/\nu^2, \qquad Pr = \nu/\chi_{\mathrm{L}}, \qquad Sc = \nu/D_L, \qquad St = \gamma\rho_s/(\rho_L c_{pL}\Delta T)$$
$$Re = \max\bigl(\sqrt{Gr}, \sqrt{|Gr_{\mathrm{d}}|}\bigr), \qquad Pe = Pr\,Re, \qquad Pe_{\mathrm{d}} = Sc\,Re$$

where β_T and β_c are the coefficients of thermal and concentration volumetric expansion; g is the gravitational constant; χ_L is the thermal diffusivity of the melt, D the diffusion coefficient in the melt, and ν is the viscosity. Thermal conductivity λ, heat capacity c_p, density ρ are non-dimensionalized by their value in the melt λ_L, c_{pL}, ρ_L:

$$\bar{\lambda} = \lambda/\lambda_L, \qquad \overline{c_p} = c_p/c_{pL}, \qquad \bar{\rho} = \rho/\rho_L$$

R_c is the crystal radius, and γ the heat of fusion. $\Delta T = 185$, the temperature drop, corresponds to the following phase change diagram: $T = 985$ K at $c = 0$, i.e. pure GaSb, and $T = 800$ K at $c = 1$, i.e. pure InSb (see Fig. 1(a)) so $\Delta c = 1$. The equations were non-dimensionalized using the following scaling factors: R_c for length; $t_o = R_c/u_o$ for time, where $u_o = \nu Re/R_c$ for the velocity. Instead of the temperature we will consider the deviation of the temperature from $T^* = 985$ K, divided by ΔT. In the melt zone the Navier–Stokes equations for an incompressible viscous liquid in which the Boussinesq approximation, written in vorticity-stream function form, is applied are:

$$\frac{\partial\omega}{\partial t} + \mathrm{D}(\psi)\omega = \frac{1}{Re}\frac{1}{r}\left[\frac{\partial}{\partial r}\left(\frac{\partial(r^2\omega)}{r\partial r}\right) + \frac{\partial}{\partial z}\left(\frac{\partial(r^3\omega)}{r\partial z}\right)\right] + \frac{Gr}{Re^2}\frac{\partial T}{r\partial r} + \frac{Gr_{\mathrm{d}}}{Re^2}\frac{\partial c}{r\partial r} \tag{1}$$

and

$$\frac{1}{r}\left(\frac{\partial}{\partial r}\left(\frac{1}{r}\frac{\partial\omega}{\partial r}\right) + \frac{\partial}{\partial z}\left(\frac{1}{r}\frac{\partial\omega}{\partial z}\right)\right) + \omega = 0 \tag{2}$$

in which the stream function and vorticity are defined as

$$u = \frac{1}{r}\frac{\partial\psi}{\partial z}, \quad w = -\frac{1}{r}\frac{\partial\psi}{\partial r}, \quad \text{and} \quad \omega = \frac{1}{r}\left(\frac{\partial w}{\partial r} - \frac{\partial u}{\partial z}\right) \tag{3}$$

The following equations for heat and mass transfer are solved in the melt zone:

$$\frac{\partial T}{\partial t} + \mathrm{D}(\psi)T = \frac{1}{Pe}\nabla^2 T, \qquad \frac{\partial c}{\partial t} + \mathrm{D}(\psi)c = \frac{1}{Pe_{\mathrm{d}}}\nabla^2 c \tag{4}$$

In the above equations, the operator for the convective terms ($\phi = \omega, T, c$) is defined as:

$$\mathrm{D}(\psi)\phi = \frac{1}{r}\frac{\partial}{\partial r}\left(\frac{\partial\psi}{\partial z}\phi\right) - \frac{1}{r}\frac{\partial}{\partial z}\left(\frac{\partial\psi}{\partial r}\phi\right) \tag{5}$$

The equation for heat conduction is considered within the area occupied by the crystal and crucible walls:

$$\bar{c}_p\bar{\rho}\frac{\partial T}{\partial t} = \frac{1}{Pe}\nabla\cdot\bigl(\bar{\lambda}\nabla T\bigr) \tag{6}$$

The temperature distribution imposed at the external boundaries is describe below. The discontinuity of the properties λ, $(c_p\rho)$, and the continuity of the heat flow are imposed at the crystal-crucible and melt-crucible boundaries:

$$[T] = 0, \qquad \left[\frac{\bar{\lambda}}{Pe}\frac{\partial T}{\partial n}\right] = 0 \tag{7}$$

Here and below, the symbol "[ ]" denotes the change of the function inside the brackets across the surface. A symmetry condition is imposed at the axis for temperature, concentration and velocity. For the melt flow at the solid

boundaries there are conditions of non-penetration and of adhesion. For the vertical velocity in the gap the condition of mass balance was imposed. At the m/c interface, the temperature is continuous. As in [4,10,14], the instantaneous solidification velocity at the m/c interface was calculated as being proportional to the supercooling of the m/c interface (the last part of Eq. (8)).

$$[T]_s^l = 0, \qquad T_*(c) = f(c), \qquad \left[\frac{1}{Pe}\frac{\partial T}{\partial n}\right]_s^l = St\, v_n, \qquad \frac{1}{Pe_{\mathrm{d}}}\frac{\partial c}{\partial n} + v_n c = v_n c_s$$
$$c_s = k(c)c, \qquad v_n = \beta\big(T_*(c) - T\big) \tag{8}$$

where $f(c)$, the phase change diagram, and $k(c)$, the segregation coefficient, depend on concentration. The coefficient of proportionality β, called the kinetic factor, is chosen as the value for rough crystallization [11], and is large, [11], so that the supercooling really is negligible (less than thousandths of one degree). As calculations had shown, the solutions are both classical Stephan problems, and the non-classical one for large kinetic coefficient values is practically identical.

The solution was obtained by the finite-difference method with a preliminary mapping of the melt areas and the solid areas into computational square blocks. A non-uniform mesh was used for all blocks. In each block, the mesh clustered near the boundaries, especially near the liquid zone boundaries [12]. An implicit conservative, monotonic, unconditionally, stable difference scheme, based on extended stencils with monotonizing regularizers of the third order was used to approximate the equations and boundary conditions [13]. The stream function, vorticity, temperature and concentration were determined for each time step. The source term depending on the interface supercooling, on the kinetic factor and on the heat of fusion has been used in the grid temperature equation at the m/c interface. Thus the temperature also was defined at the m/c interface. The m/c interface velocity was calculated with use of the kinetic factor and of interface supercooling. Thus, a new m/c interface position was also calculated.

Due to the transformation of the physical domain into a mathematical region consisting of unit squares, the explicit tracking of the m/c interface has always a constant number of non-uniform grid nodes in each square. The mesh is condensed to the boundary of each region, so the melt boundary layer is always covered by a fine mesh. By using additional fixed-sign regularizers, convective terms became monotonic. This regularizer prevents the appearance of grid oscillations in time [13]. It contains approximations of fourth derivatives with the factor $O(h^3)$ (where h is a step with respect to the spatial variables) and eliminates 'sawtooth' solutions with respect to r and z. Total supplementary dissipation of a solution has the order of h^3. The regualizer's values are really small in the boundary melt layer even for large changes in the melt velocity, because the spatial step in the boundary layer is chosen very small. Far from the m/c interface, the regularizer's values are also small due to small changes in the melt movement velocity in these zones. Therefore, the grid steps are chosen small closed to boundaries, particularly to the melt/crystal interface, and bigger far from boundaries. Thus, the total number of grid nodes can be chosen sufficiently small. The limitation on the time step depends only on the physical problem [13]. In the present article, as in [4,10,14], all equations are combined into two algebraic systems. One of these contains the temperature and concentration equations together with boundary conditions and conditions given by Eq. (8). A second contains the equations for vorticity and stream functions. This is unlike the numerical method of work [12], where three systems of equations, temperature, concentration, vorticity and stream function, were considered. The Gauss method was applied to solve the systems of algebraic equations, nonlinear terms were taken from previous time step. The combination in one system of Eqs. (4), (6)–(8) and of boundary conditions (the non-classical Stephan problem consideration) is very useful from a numerical point of view as this scheme may be applied to crystal growth problems regardless of which melt crystal growth occurs: pure alloys, or dopant melt, or binary ones. This approach has become a more stable solution than it was in [12]. Also this numerical method enables one to solve the facet crystal growth problem, based on the mathematical model and the method from [9].

For numerical modeling a grid with 61 nodes in the z-direction was chosen, including 43 points in the liquid zone. The grid step was equal to 0.001 in the boundary layer. Far from the m/c interface it was increased to 0.03. Along radius a non-uniform grid was chosen, with 22 points.

4. Numerical results

Calculations were performed for a crystal radius $R_c = 10$ mm and $R_c = 30$ mm, a graphite crucible thickness equal to 2 mm, and the thickness of AHP-heater bottom of 2.8 mm. The initial seed height was equal to 15 mm. The seed

composition was chosen small ($c_s = 0.02$), because of the difficulty of having a high crystal composition (and it is very expensive). The initial height of the $W1$ zone H was equal to 5 mm. The pulling velocity was assumed $V = 1$ and 3 mm/h (the last value is close to the value used in [1]). The initial melt composition: $c_1 = 0.3$, $c_2 = 0.06$. The initial position of the T6 point was equal to the initial seed position, 15 mm. At this point the temperature corresponded to a liquid concentration, c_1, in accordance with the phase change diagram: T6(0.3) = 944.46 K, Fig. 1(a). The temperature along the crucible side wall was changed with a gradient of 60 K/cm (this is a parameter value close to that from the experiment described in [1]). After one hour stationary ($V = 0$) the AHP-heater was moved up, the points (Fig. 1(c)) T7, T6, T5 (the last one was below T6 at 10 mm) moved with the same velocity. Upper temperatures $T1 = T2 = T7$, temperatures T6 and T5 were not changed in time, $T3 = T4$, and was changed in time according to the side wall temperature gradient, because the crystal length was changed due to its growth. The following parameters were used for the Bridgman growth: $R_c = 10$ mm, $V = 1$ and 3 mm/h, $c_s = 0.02$, $c_1 = 0.06$, melt length $H = 200$ mm.

Concentration distributions in the crystals grown for different test case problems are presented in Fig. 2. The black curves are the axis distribution, the blue ones, the side wall. The curves obtained at $V = 1$ mm/h and at different radii $R_c = 10$ mm, 30 mm by the AHP-method were marked by '1' and by '2' respectively in Fig. 2(a). The curves obtained at $V = 1$ mm/h and at $R_c = 10$ mm by the Bridgman method were marked '3' (Fig. 2(a)). The grown crystal composition for the fourth case ($V = 3$ mm/h and $R_c = 10$ mm, AHP-growth, '4') and for the fifth case (the same as fourth one but without solute convection ($Gr_d = 0$), '5') are shown in Fig. 2(b). The sixth case corresponds to the Bridgman growth at $V = 3$ mm/h and $R_c = 10$ mm, see Fig. 2(c).

During the holding process the seed was melted a little; therefore the melt composition always was decreased at the beginning. The grown crystal composition reached stationary regime in the cases of AHP-growth (curves marked '1', '2', '4', '5', Fig. 2). Furthermore, the r-average crystal composition is exactly equaled to the desired 0.06 value at the stationary regime. This fact is a result of the mass balance: if a melt with c_2 composition flowed through the gap into the melt it should be solidified after some transient process. The preparation of a rich concentration zone $W1$ close to the m/c interface helps to reduce this transition time significantly, with the AHP-heater assisting. For an equal initial concentration in both zones $W1$ and $W2$ ($x = 0.06$) the transition time is increased significantly, but a stationary regime also exists. From Fig. 2 it is clear that the AHP-method always results in the growth of high concentration crystals. In the third case (the Bridgman technique) the crystal grown at small pulling velocity (1 mm/h) has a small concentration up to 80 mm. For the sixth case at $V = 3$ mm/h the grown crystal composition (Fig. 2(c)) became very large and lateral scatter α is more than 70%, where $\alpha = 100\%(c_{\max} - c_{\min})/(c_{\max} + c_{\min})$. The m/c interface becomes concave inside the crystal and its radius is huge too, more than 10 mm. This is similar to results in [1]

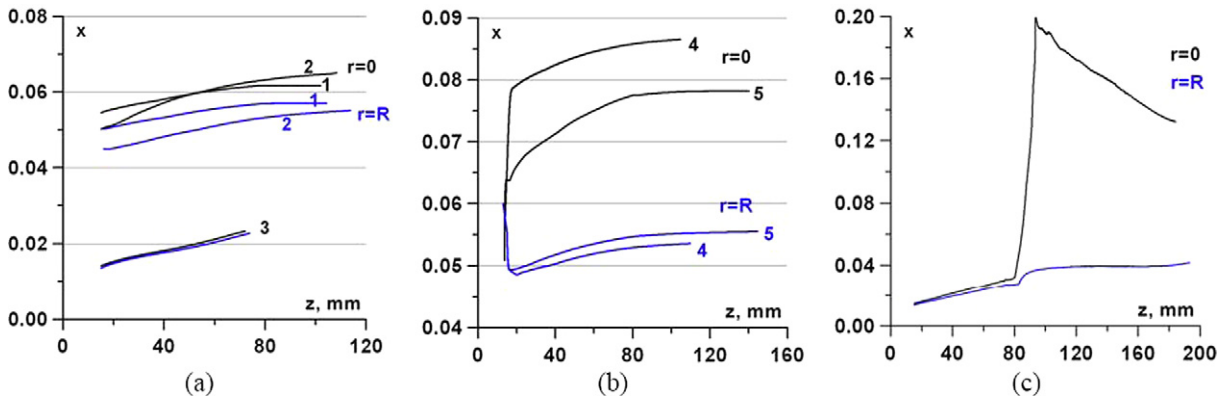

Fig. 2. The concentration distributions in the grown crystal at the axis (black curve) and the side wall (blue one): (a) first and second cases (called '1' and '2') were obtained during AHP growth at $V = 1$ mm/h and $R_c = 10$ mm and at $R_c = 30$ mm, respectively, third case—Bridgman growth at $V = 1$ mm/h and $R_c = 10$ mm ; (b) fourth and fifth cases—AHP-growth at $V = 3$ mm/h and $R_c = 10$ mm with and without solute convection; (c) sixth case—Bridgman growth at $V = 3$ mm/h and $R_c = 10$ mm.

Fig. 2. Champs de concentration dans le cristal au niveau de l'axe (tracé noir) et à la paroi (tracé bleu) : (a) les premier et second cas (marqueurs « 1 » et « 2 » resp.) sont obtenus durant la croissance AHP à $V = 1$ mm/h, $= 10$ mm et $= 30$ mm resp., troisième cas—croissance de Bridgman à $V = 1$ mm/h et $= 10$ mm ; (b) quatrième et cinquième cas—croissance AHP a $V = 3$ mm/h et $= 10$ mm avec et sans convection solutale ; (c) sixième cas—croissance de Bridgman à $V = 3$ mm/h et $= 10$ mm.

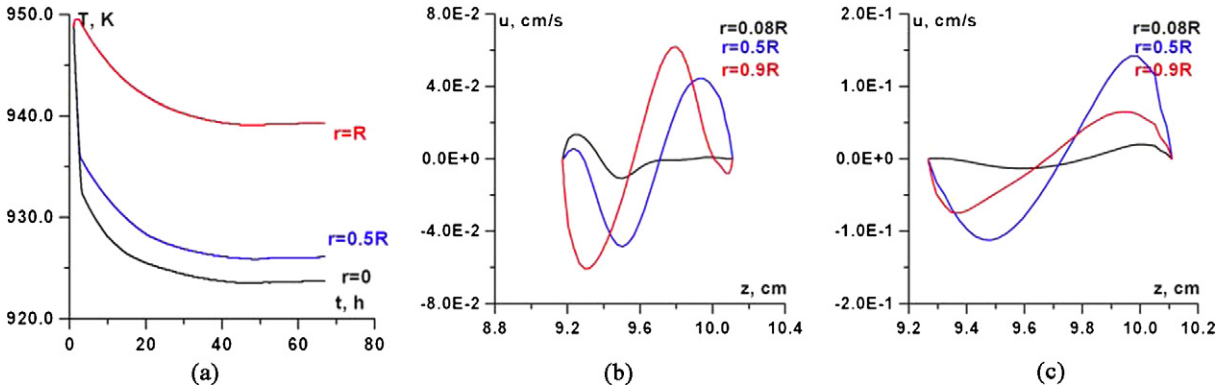

Fig. 3. (a) Time dependence of interface temperature for fourth case (AHP, $V = 3$ mm/h, $R_c = 10$ mm); (b) and (c) z-distribution of radial component of flow velocity close to the axis ($r = 0.08R_c$, black curve), at half radius (blue) and close to side wall (red) for fourth (b) and fifth (c) cases (with and without solute convection).

Fig. 3. (a) Évolution de la température de l'interface pour quatre cas (AHP, $V = 3$ mm/h, $= 10$ mm) ; (b) et (c) variation selon z de la composante radiale de vitesse au voisinage de l'axe ($r = 0, 08$, tracé noir), à mi-rayon (bleu) et proche de la paroi (rouge) pour quatre (b) et cinq (c) cas (avec et sans convection solutale).

for $x = 0.06$. Such a coincidence is not accidental: growth conditions (composition, temperature gradient, cooling velocity) are close to the experiment. Further lateral concentration scatters were calculated at $z = 90$ mm of grown crystal for test case problems of AHP-growth. The smallest lateral scatter is 4% and corresponds to first case, to smaller velocity. With increasing of pulling rate up to 3 mm/h the $\alpha = 23\%$ (Fig. 2). In [7,8] the pulling velocity was less than 1 mm/h. With an increasing crystal radius, the scatter is increased too. At $R_c = 30$ mm $\alpha = 8.6\%$, which is really good, especially for such a large crystal radius.

Interface concavity inside the crystal for cases of AHP-growth was small for the first variant ($V = 1$ mm/h, radius 10 mm). The concavity was equal to 2.5 mm. At a higher velocity (3 mm/h, the fourth case) and the same radius, 10 mm, it was equal to 5 mm. Increasing the internal radius by a factor of three at a small pulling rate 1 mm/h (case 2) lead to doubling of the interface concavity to 5.5 mm. Fig. 3(a) presents the time-dependence of the m/c interface temperature for the fourth test case problem, which had the biggest concentration scatter. The temperature drop amounted to 26 K along the m/c interface. For the other cases this value was smaller.

Figs. 3(b) and (c) present distributions of radial component of flow velocity u_r along z-direction at different values of $r = 0.08R_c$ (black curves), $r = 0.5R_c$ (blue curves), $r = 0.9R_c$ (red curves), obtained for the fourth and the fifth test case problems ($t = 28$ h). Due to solute convection, the intensity of flow movement decreased at least twice (compare Fig. 3(b) and (c)). Thus the concentration distribution of grown crystals had bigger lateral scatter (see Fig. 2(b)). The velocity distributions at $r = 0.8$ mm and at $r = 5$ mm had positive values. This infers that there is a small vorticity near the axis and the m/c interface, where the melt moved from the axis. As calculations indicated, this vorticity is unstable, and at times it disappeared. In the whole flow, convection is sufficient for melt mixing. For the sixth test case problem (Bridgman growth, 3 mm/h) u_r has maximum value ~ -0.0008 cm/s close to the m/c interface (boundary layer) and it was much smaller inside the melt. The convection motion was really stagnant. It is not surprising that there is such a huge radial concentration scatter, Fig. 2(c). The diffusion coefficient is very small as the melt concentration is very high. So both mechanisms, diffusion and convection, could not mix the highly concentrated boundary layer. For this Bridgman growth problem, the boundary temperature condition is an idealization of condition from [1], constant in time. So here the intensity of flow convection for the sixth case is smaller than that obtained in [4] for experiment [1]. In [4] the maximum value of radial component of flow velocity was smaller by a factor of four, (less than 0.01 cm/s) than in the fourth case. As it was shown numerically that [4] there was a stagnant layer close to m/c interface whose length was ∼20 mm. Above this layer there was an intensity vorticity caused by the changing of the side wall temperature gradient at the junction of the crucibles made of different materials, [1]. When the m/c interface came to this point, a strong convection flow mixed the concentration in this stagnant zone and homogeneous growth continued ($x = 0.06$, [1] and [4]).

5. Conclusions

This article discusses the results of the mathematical modeling of $In_xGa_{1-x}Sb$ growth by AHP and by Bridgman methods. Test case problems having some idealized conditions close to real experimental data were used. Numerical modeling for the Bridgman test case crystal growth problem illustrated that it would be impossible to grow homogeneous crystals of high composition even with very small diameters. This was demonstrated experimentally in [1]. The mathematical modeling performed on $In_xGa_{1-x}Sb$ growth by the AHP method indicated the possibility of producing a very homogeneous crystal of large diameter and high composition. Submerged into the melt, the AHP-heater acts as a barrier: the crystallization zone is limited by the m/c interface and the bottom of the AHP-heater. The AHP-heater is an essential technological detail which influences the growth process. This technique produces a small crystallization zone close to the interface. The physical state of this zone (temperature, composition, velocity field) could be easy described, so it is possible to produce the changes needed in order to manage the crystal growth process. In the present article, the complex convection caused by temperature and concentration drops in the melt was still sufficient for adequate melt mixing in spite of the small diffusion coefficient at high concentrations (AHP-growth). Due to possibility of preparing the initial composition for the crystallization zone $W1$, the time to reach the quasi-stationary regime could be reduced. It was shown that reducing the pulling rate, the radial concentration scatter could be significantly decreased. Numerical simulations of various test case problems together with real experimental data have indicated that good quality crystals of large diameter could be grown by the AHP-method.

References

[1] N. Duhanian, T. Duffar, C. Marin, E. Diegez, J.P. Garandet, P. Dantan, G. Guiffant, Experimental study of the solid–liquid interface dynamics and chemical segregation in semiconductor alloy Bridgman growth, Journal of Crystal Growth 275 (2005) 422–432.
[2] I. Ansara, M. Gambino, J.P. Bros, Journal of Crystal Growth 32 (1976) 101.
[3] C. Stellian, T. Duffar, Numerical analysis of solute distribution and interface stabilization during experimental Bridgman growth of concentrated GaInSb alloys, Journal of Crystal Growth 275 (2005) e585–e594.
[4] M. Marchenko, T. Duffar, Numerical study of boundary condition influence on convective flow and heat/mass transfer during concentrated alloy Bridgman crystal growth, in: 13th International Heat Transfer Conference, Sydney, Australia, 2006, submitted for publication.
[5] A. Ostrogorsky, US Patent Application S.N. 397741, 1989.
[6] V. Golyshev, M. Gonik, Patent of RF # 180085415, 1990.
[7] S. Bykova, V. Golyshev, M. Gonik, V. Tsvetovsky, M. Marchenko, I. Frjazinov, T. Duffar, Investigation of conditions for homogeneous $Ga_{1-x}In_xSb$ crystals growth under conditions of weak melt flows, J. Crystallography 49 (2) (2004) 369–375 (in Russian).
[8] S. Bykova, V. Golyshev, M. Gonik, V. Tsvetovsky, M. Marchenko, I. Frjazinov, T. Duffar, Investigation of conditions for homogeneous $Ga_{1-x}In_xSb$ crystals growth under conditions of weak melt flows, in: Proceeding of the 5th Int. Conference on Single Crystal Growth and Heat & Mass Transfer, vol. 1, Obninsk, Russia, 22–26 September, 2003, pp. 101–108.
[9] V. Golyshev, M. Marchenko, I. Frjasinov, Effect of boundary temperature conditions on the shape of the phase interface, on melt flow and impurity distribution during the growth of single crystals by the AHP-method, in: Proc. 4th Int. Conf. on Single Crystal Growth and Heat & Mass Transfer, vol. 3, Obninsk, Russia, 24–28 September, 2001, pp. 715–724.
[10] M. Marchenko, Numerical study of low frequency oscillation appearance during $In_xGa_{1-x}Sb$ crystal growth by Bridgman and AHP methods, in: A.J. Nowak, R.A. Bialecki, G. Wecel (Eds.), Eurotherm Seminar 82, in: Numerical Heat Transfer, vol. 3, ISBN 83-922381-2-5, 2005, pp. 703–712.
[11] A. Chernov, E. Givargizov, et al., Modern Crystallography, vol. 3, Nauka, Moscow, 1980 (in Russian).
[12] M. Marchenko, I. Frjazinov, Computer code CARMA1 for solving nonstationary problem of crystal growth in ampoule, Journal of Computational Mathematics and Mathematical Physics 37 (8) (1997) 988–998.
[13] I. Frjazinov, M. Marchenko, O. Mazhorova, Monotone corrective terms and coupled algorithm for Navier–Stokes equations of an incompressible flow, Journal of Mathematical Modelling 6 (N12) (1994) 97–116 (in Russian).
[14] M. Marchenko, Use of uniform algorithm for heat and mass transfer during directional crystallization both from dopant and from binary melt, in: Proceedings of 4th ICCHMT May 17–20, 2005, Paris-Cachan, France, ICCHMT'05, paper-426.
[15] M. Marchenko, I. Friazinov, Mathematical model and numerical realization of faceted crystal growth process, Crystallography Reports 50, N6, pp. 1114–1122.